Characterization of localized hole states in Pr$_{1+x}$Ba$_{2-x}$Cu$_3$O$_{6+y}$ by nuclear magnetic resonance

M. W. Pieper*

TU-Wien, Wiedner Hauptstraße 8, A-1040 Wien, Austria

F. Wiekhorst

Universität Hamburg, Jungiusstraße 11, D-20355 Hamburg, Germany

T. Wolf

Forschungszentrum Karlsruhe, Institut für Technische Physik, Universität Karlsruhe, D-76128 Karlsruhe, Germany

We investigated the charge distribution in Pr$_{1+x}$Ba$_{2-x}$Cu$_3$O$_{6+y}$ crystals at liquid-He temperature by means of ^{63,65}Cu and ^{141}Pr-NMR and nuclear quadrupole resonance. The electric-field gradients determined for the different oxygen coordinations of Cu(1) on the chains confirm the model that the hole states are localized in the O2$p\pi$ orbitals of the CuO$_2$ planes. The intensity and line-shape analysis of the Cu(1) and Pr resonances in the oxygen doping series ($x \approx 0, y = 0 \cdots 1$) and in the Pr/Ba solid-solution series (at $y = 1$) allows us to assign the Pr resonance to Pr at rare-earth (RE) sites. Therefore we can investigate the charge distribution in the CuO$_2$-Pr-CuO$_2$ layers by crystal-field analysis of the Pr signal. To consistently describe our results with neutron-scattering data we propose that two Pr states are present in the RE layer, and ascribe them to Pr with and one without a hole localized in the oxygen coordination shell. NMR detects only the former, with a virtually nonmagnetic singlet ground state, while space-integral techniques are dominated by the latter, due to a quasidoublet ground state and antiferromagnetism of its Pr moments at low temperature.

I. INTRODUCTION

PrBa$_2$Cu$_3$O$_7$ is the one insulating member of the isostructural series REBa$_2$Cu$_3$O$_7$ of high-T_c superconductors[1] (RE =rare earth, Y, La, abbreviated below RE123). Simultaneously the magnetic properties of Pr differ dramatically from the reasonably well understood 4f magnetism of all other rare earths in this structure. This extraordinary behavior of Pr attracted considerable interest from experimental and theoretical physics throughout the last decade because it might shed some light on the microscopic origin of high-T_c superconductivity in the cuprates. From the point of view of applied physics it is important to understand the physical properties of the material because of its potential use in superconductor-insulator heterostructures.

There is a general consensus that the structural key element of the cuprate superconductors are the CuO$_2$ planes. The undoped CuO$_2$ plane is an antiferromagnetic charge-transfer insulator: Photoemission spectroscopy shows that the on-site correlation energy of the Cu-$d_{x^2-y^2}$ electrons is large enough to push the lower Hubbard band below the 2p-oxygen band.[2] Upon hole doping an insulator-metal transition (MIT) takes place, with a superconducting ground state in a certain range of hole concentrations. The dependence of the superconducting transition temperature T_c on the hole concentration n_h in the CuO$_2$ plane follows a universal law close to $T_c/T_{cmax} = 1 - [(n_h - n_{opt})/\Delta_n]^2$, where this has positive solutions[3,4] (note that other dependencies have been proposed, e.g., the trapezoid shape in Ref. 5). In contrast to the large differences in the maximum transition temperature T_{cmax} between cuprates, the variations of the optimum hole concentration $n_{opt} \approx 0.3$/CuO$_2$ unit and the threshold concentration Δ_n for superconductivity appear to

be rather small. The fact that Pr123 is an antiferromagnetic insulator instead of metallic and superconducting like the other members of the RE123 series may then be due to either a suppression of the doping, or a detail of the electronic structure lowering T_{cmax} dramatically.

There is no obvious and generally accepted parameter connected with T_{cmax} of the cuprates. In RE123 one finds nearly independent of the RE $T_{cmax} = 93 \pm 4$ K. Magnetic pair breaking by the Pr-4f moments, enhanced by a hybridization with the bands in the CuO$_2$ planes, has been invoked as a mechanism to suppress superconductivity by lowering T_{cmax}. A phenomenological combination of Abrikosov-Gorkov pair breaking and hole depletion can successfully describe the dependence of the superconducting T_c on the Pr concentration in Pr$_z$RE$_{1-z}$123,[6,7] and it has been argued that the exceptionally high ordering temperature of the Pr sublattice, $T_N = 12$–18 K compared to 2.1 K for Gd, also supports this view.[8] However, the results cannot be described by pair breaking alone, it is necessary to take hole depletion into account. Otherwise Pr would not suppress superconductivity and the MIT at the same critical Pr concentration, and T_c would drop linearly at small z, which is not observed.[7,6,9] Furthermore, there is evidence against pair breaking,[10] and it is possible to model $T_c(z)$ without magnetic pair breaking under the assumption that the influence of Pr on the doping depends on its concentration.[9,11] Even if one agrees that pair breaking is indicated experimentally at least near the critical Pr concentration, it is not obvious that a Pr moment is involved since near the MIT localized Cu moments in the CuO$_2$ layers may be candidates for pair breakers as well.

Therefore the current attempts to explain the role of Pr focus on the suppression of the hole doping. There is clear

experimental evidence that Pr does not simply fill the hole states with its $4f$ electrons. Various techniques,[12–14] including inelastic neutron-scattering (INS) (Refs. 15 and 16) and our own previous NMR work,[17,18] show that the valence of Pr is close to 3, the same as for the other RE, and stays constant independent of the oxygen content x.[19] Furthermore, spectroscopic methods sensitive to the density of O-$2p$ hole states detect similar amounts in Pr123 as in the other RE123.[20,21]

The by now generally accepted model for the suppression of hole doping was proposed by Fehrenbacher and Rice (FR). In their model the holes become localized in the antibonding O-$2p\pi$ orbitals of the planes.[22] These states are favorable to the $2p\sigma$ states populated in the absence of Pr due to their hybridization with the $4f^2$ shell of Pr. This view has been supported and extended by band structure calculations of Liechtenstein and Mazin, showing that with increasing radius of the RE just for Pr a different band with $4f$ character crosses the Fermi level,[23,24] and by Wang, Rushan, and Su, who explicitly included a third band from the chain layers to describe the hole concentration as a function of the Pr concentration in the RE layer.[11] As an alternative to the hybridization models it has been discussed that Pr might push the hole states in a band associated with the apex oxygen.[25,26]

Experimentally, the hybridization shows (among other techniques) in detailed Pr-O bond-length analysis,[27] in the strong broadening of the crystal-field transitions in INS,[15,16] and x-ray absorption.[28,29] Using polarized x rays Merz et al. were recently able to show that the orientation of the $2p$-hole states in the structure is indeed different in Y123 and Pr123, giving very strong support to the hybridization model.[30] Clearly, a microscopic characterization of the localized hole states is very desirable in order to distinguish between the models and address open problems such as the mechanism of the carrier localization or of the role of the Pr and Cu magnetism at low temperature.

In RE123, doping of the CuO_2 planes is achieved by variation of the oxygen content of the chain layer, and one of the basic ingredients of hybridization models is that this doping mechanism is independent of the RE ion. A model for the dependence of the hole count n_h on the oxygen concentration in the chains y has to address two problems, namely, the distribution of oxygen in the chains, and the hole count induced by a given oxygen configuration.[31] The nonrandom oxygen distribution in the chain layer is best described by the asymmetric next-nearest-neighbor Ising model.[32,33] It describes the various superstructures observed at intermediate y (most important the formation of chains in Y123 at $y=0.5$) which depend strongly on the RE ion. Lütgemeier et al. have shown that Cu(1)-(chain-)site NQR is a suitable method to investigate this distribution,[34,35] but they did not include Pr123 in their studies, so we analyze this case below in some detail.

The dependence of the hole count on the oxygen configuration with the chain length as the most prominent parameter has been subject to detailed theoretical studies in Y123.[36,26] On the experimental side the electric-field gradient (EFG) at the Cu(1) sites is a sensitive probe of the charge balance between the planes and the chain layer.[37] Ohno, Koyama, and Yasuoka used this to estimate the number of mobile carriers in the planes of metallic, fully oxidized $Pr_zY_{1-z}123$.[38] Below we use the Cu(1) EFG at various oxygen contents to verify experimentally the assumption underlying the FR model, that the CuO chains dope holes into the CuO_2-RE-CuO_2 layers, independent of the presence of Pr.

One might expect that the special arrangement of charges in the hybridized state proposed by Fehrenbacher and Rice shows in the crystal-field parameters of the $4f$ shell of Pr. Unfortunately, the lines from crystal-field transitions in INS are severely broadened, giving rise to large uncertainties in the symmetry as well as in the energies of the low-lying crystal-field levels.[15,16] NMR is very sensitive especially to the symmetry of the ground state and the position of the lowest excitations.[39] In a previous work we reported measurements of the ^{141}Pr resonance in Pr123 for $y=1$.[18] Most remarkably, we found a different ground-state symmetry for Pr^{3+} from the one used to describe the INS spectra. Moreover, the virtually nonmagnetic state of Pr at low temperatures which is without doubt what is observed in our NMR measurements is in clear contrast to the antiferromagnetic Pr order detected by neutron diffraction and the homogeneous susceptibility.[40–42,8]

Our interpretation of the NMR data has been strongly questioned because of these findings,[43,41,8] but no consistent explanation for both the NMR and the neutron data has been proposed up to now. Therefore we extended the investigation of the Pr resonance to crystals over the whole range $y=0-1$ of oxygen concentrations, and to crystals with different concentrations in the Ba/Pr solid-solution system. On this basis we confirm our initial assignment of the Pr resonance to Pr on regular RE sites. In view of the strong doubts our brief description of the $4f$ ground state in Ref. 18 did encounter we give below a rather detailed discussion of our determination of the crystal-field ground states of Pr in this structure. This leads us to a consistent description of the NMR and neutron experiments, basically by assuming that the interpretation of both has been correct, and assigning two different electronic states of Pr to the conflicting experimental observations.

Finally we discuss the impact of this model on the understanding of the low-temperature magnetism of Pr and the other rare earths in this remarkable material. As indicated above, the Pr magnetism with its Néel temperature up to 18 K in Pr123 and in related cuprates[40,44–47] is as outstanding as the suppression of superconductivity. It is tempting to relate the two effects by the argument that the $4f$-$2p\pi$ hybridization suppresses superconductivity by switching on pair breaking at Pr moments, and simultaneously induces the high T_N via a substantial enhancement of the $4f$-$4f$ exchange.[8] We would like to caution about this argument: While there is ample evidence for the hybridization itself and we present more below, the contribution of pair breaking to the suppression of superconductivity is much less clear (see above), and the role of the $4f$ exchange in Pr magnetic order seems even more open. In fact the exchange is known to be small for all other rare earths, the ordering of the other $4f$ moments is mostly due to dipolar interactions.[48] This is most convincingly demonstrated by the small dependence of T_N on magnetic dilution in the rare-earth sublattice for all magnetic RE ions.[49–51] All magnetic RE, including the exceptional singlet ground-state Pr, order well above the 40% percolation threshold for dilution of the square lattice with nearest-

neighbor exchange. The order is therefore ascribed to the long-range dipolar coupling of the magnetic rare earths, which is clearly not an option in the case of Pr123. The dependence of T_N on oxygen content is also puzzling, if hybridization enhanced exchange is the origin. At $y=0$, where there is no hybridization of hole states, T_N is still as high as 12 K. In Pr123, T_N increases with the hole count, while it decreases for Nd in Nd123.[48] In the concluding section of the discussion we show that the increase of T_N of Pr is even more puzzling in view of our NMR data, and discuss induced magnetism of the Pr sublattice as an alternative model.

II. EXPERIMENTAL DETAILS AND RESULTS

A. Sample characterization

The main difficulties in the experimental verification of the models arise from the complex doping mechanism in the RE123 series on the hand, and from the strong influence of crystal preparation on the material properties on the other. A remarkable example is the preparation of crystals under special conditions that do become superconducting, with T_{cmax} even higher than in the other RE123 (>100 K under pressure).[52,53] In order to provide a reliable basis for comparison of results obtained with other samples we present in this subsection a rather detailed description of the sample preparation.

High quality Pr123 crystals of a size suitable for NMR ($\geqslant 10$ mg) are still very difficult to prepare. One major problem is the contamination of the Cu(1) sublattice with Al from Al_2O_3 crucibles (up to 30%), because this has a strong influence on the oxygen distribution[54] as well as on the magnetic structure of the Cu(2) sublattice at low temperature.[55] We avoid the Al contamination by use of MgO crucibles, which results in a much smaller contamination by Mg ($\approx 1\%$) because of the higher melting point of MgO.[56] The best stoichiometric crystals available are grown in $BaZrO_3$ crucibles, but they have been too small for NMR up to now.

A second problem is the existence of a finite solid solution range for the RE/Ba sublattices for the light rare earths (Nd, Pr, La).[57-60] The solid solution range is a four-dimensional volume in the phase diagram spanned by temperature T, partial oxygen pressure $p(O_2)$, and the two-dimensional (2D) triangle of cation concentrations, sketched for fixed T and $p(O_2)$ in Fig. 1. The stable compositions form the surface of this volume in the phase diagram with the ellipses in Fig. 1 (top) indicating cross sections. Also shown are the liquidus surfaces and the conoidal lines connecting them to the solid solution systems at two different $p(O_2)$. In the absence of other metals which may substitute for Cu (e.g., Al from the crucibles) one may assume a constant Cu content. In this case the ellipses in Fig. 1 degenerate to horizontal lines at the concentrations $RE_{1+x}Ba_{2-x}Cu_3O_{6+y}$, and the solid solution range has only the three degrees of freedom T, $p(O_2)$, and x.

The accessible range of x depends on temperature, oxygen partial pressure, and on the rare-earth radius. In general, the RE content x increases with increasing oxygen partial pressure and rare-earth radius, and with decreasing temperature, at least in the vicinity below the peritectic temperature. We grew Pr123 crystals by the slow cooling method.[61] The Pr/Ba
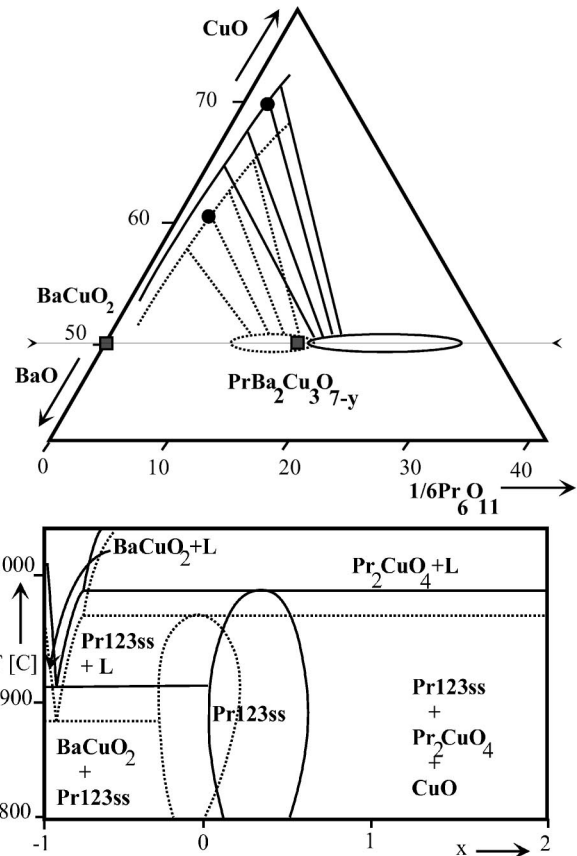

FIG. 1. Top: Schematic phase diagram of the Pr-Ba-Cu-O system at 940 °C in 1-bar O_2 (solid lines) and in 63-mbar O_2 (dotted lines). Stoichiometric phases are indicated by filled squares. A few conoidal lines connecting the liquidus surface with the Pr/Ba solid solution system (Pr123ss) are shown with the starting compositions for the crystal growth marked by the dots. Bottom: Schematic phase diagram along the horizontal line corresponding to $Pr_{1+x}Ba_{2-x}Cu_3O_{7-y}$ in the upper part, again for 1-bar O_2 (solid), and 63-mbar O_2 (or 300-mbar air, dotted).

ratio of the growing crystals was set by the Cu/Ba ratio of the flux via the conoidal line to the solidus surface. Temperature and oxygen pressure for variations of x were chosen as marked by the dots in the phase diagram to obtain crystals with high and low Pr content along the conoidal lines indicated in the figure (see also Table I).

The two crystals prepared to obtain off-stoichiometric x were oxidized in 1-bar flowing oxygen in the temperature range 600–300 °C to obtain $y=1$. The crystals of the series with various oxygen content were prepared along the route denoted $x=0$ in the table, the oxygen content was set in a similar tempering step under suitable oxygen pressure. The oxygen concentration y expected from the tempering conditions is in all cases in accord with the relative NMR-line intensities of the Cu(1)-O coordinations in the chains (see below). The error in y estimated from the NMR spectra is 5%. We expect that we may not reach the end members (especially $y=0$) by approximately that margin, but will nevertheless denote them for brevity with $y=0$ and $y=1$, respectively. We did not succeed to prepare superconducting Pr123 along this route, all samples are semiconducting.

TABLE I. Preparation parameters and characterization of the crystals. The flux composition is given in the first block, followed by the preparation atmosphere and the temperature program, with a slow decrease at the indicated rate in the given interval, and a quench or slow cooling to RT. The morphology and possible growth twins are indicated in the last block.

	$x<0$	$x=0$	$x>0$
at. % Pr	2	2	2
at. % Ba	37	30	28
at. % Cu	61	68	70
	300-mbar air	1-bar air	1-bar O_2
[°C]	$970 \rightarrow 906$	$1000 \rightarrow 939$	$1000 \rightarrow 948$
[°C/h]	-0.4	-0.5	-0.35
	quench	slow cool	quench
	orthor.	orthor.	tetr.
(100)/	(010)	(010)	(111)

At this point we would like to note that the local Pr/Ba ratio of a given sample with fixed overall x can be influenced by an additional heat treatment at higher temperature as well, but the composition of the resulting crystal is inhomogeneous. For small deviations from the equilibrium surface a crystal may decompose into a member of the solid solution system with a different RE/Ba ratio, and either other stable phases like $BaCuO_2$, or a second member of the solid solution system. Larger deviations from equilibrium may lead to a spinoidal decomposition where, for example, the Pr/Ba ratio varies laterally and changes with time. The final state of these decomposition reactions depends on the initial RE/Ba ratio and whether or not this cation ratio is located inside the four-dimensional volume of the solid solution system. In the case of a spinoidal decomposition the regions of different Pr/Ba ratios within a sample are very close to each other (10–100 nm), and any integral chemical analysis will reproduce the composition of the untreated sample.

Unfortunately, the substitution of Ba by Pr (abbreviated $[Pr]_{Ba}$ below) is hard to detect by standard scattering techniques because of the similar scattering cross sections of Pr and Ba. We have therefore up to now in our preparation little quantitative control of x. A unique way to determine the $[Pr]_{Ba}$ concentration is the magnetic signal in polarized neutron scattering from these defects.[62] Crystals prepared along the route denoted $x=0$ were analyzed by Markvard et al. using this technique, and a $[Pr]_{Ba}$ concentration near 5% was detected.[63] We therefore expect $x \approx 0.05$ in the crystals we tempered to obtain various oxygen contents.

Neutron diffraction showed that Pr on Ba sites is not responsible for the extraordinary suppression of superconductivity in Pr123. Kramer et al. report that $[Pr]_{Ba}$ and $[Nd]_{Ba}$ have similar influence on the materials properties.[64] The RE ion binds oxygen on otherwise empty neighboring O(5) oxygen sites between chains, disrupting the chain order in the process.[65] The defect is expected to reduce the hole count in the planes and provides a strong scattering center in the chain layer, where it may contribute to suppress one-dimensional (1D) conductivity in the chains.[66–68] However, the experiments indicate that the influence of the defects is limited to the chains, an independent mechanism not active in Nd123 must be present in Pr123 to suppress the MIT and superconductivity in the CuO_2 planes.[69] We emphasize, however, that $[Pr]_{Ba}$ may well influence the low-temperature magnetic structure of the Cu(2) sublattice by inducing magnetic moments on Cu(1) sites.[70,71] NMR and neutron diffraction consistently showed that Cu(1) moments induced by (nonmagnetic) Al couple the planes ferromagnetically along the c axis and can induce a rotation transition of the Cu(2) moments (AF-II structure) to avoid Cu(1) frustration.[72,55] A similar magnetic transition in Al free, semiconducting Nd123 may well be due to Nd on Ba sites,[48,73] and Rosov et al. reported ordered Cu(1) moments in Pr123 at low temperature.[74] Magnetic Cu(1) is not detected in Cu(1) NQR (see below and Ref. 75) and is therefore most probably localized at defect sites in the structure.

While x is always positive for Nd, the accessible range in the Pr/Ba solid solution system may extend to the Ba-rich side, as is the case for La/Ba in La123.[59,27] Substitution of Pr (+3) by Ba (+2) should increase the hole count in the planes, and, in fact, it has been suggested that the superconductivity in Pr123 crystals prepared by Zou and co-workers[76,52,77] might be due to heavy Ba doping of the Pr sublattice.[52,78] Note that disorder on the Pr sublattice at smaller defect concentrations has been invoked as a viable mechanism to localize the hole states in the $4f$-$2p$ π-hybridization band.[23]

The symmetry and the morphology of the oxidized crystals depend in a characteristic way on x that we also find in La123 and Nd123. Ba-rich and stoichiometric crystals exhibit an orthorhombic structure with twins, whereas the Pr-rich crystal kept its tetragonal structure even after additional oxidation treatments under high oxygen pressures. This result was expected because the extra oxygen ions on the O(5) sites between the Cu(1)O chains reduce the orthorhombicity. The morphology of the crystals changes with increasing RE/Ba ratio from isometric blocks, sometimes with additional (101) faces, formed by stoichiometric samples, to the
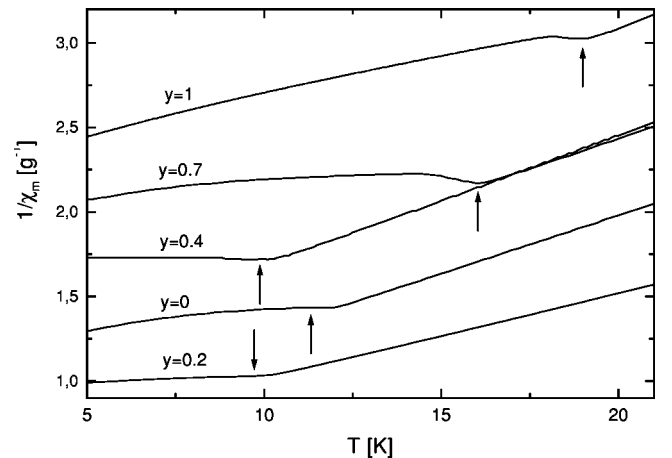

FIG. 2. Inverse low temperature a,b-plane mass susceptibilities showing the low-temperature magnetic transition. The Cu(2) sublattice orders antiferromagnetically near room temperature. Below T_{N2} (arrows) Pr carries a moment of 0.3–0.9μ_B.[79,40,41] The transition is very sensitive to sample quality; Uma et al. observed a transition in two steps in high-purity crystals grown in $BaZrO_3$ crucibles.[42]
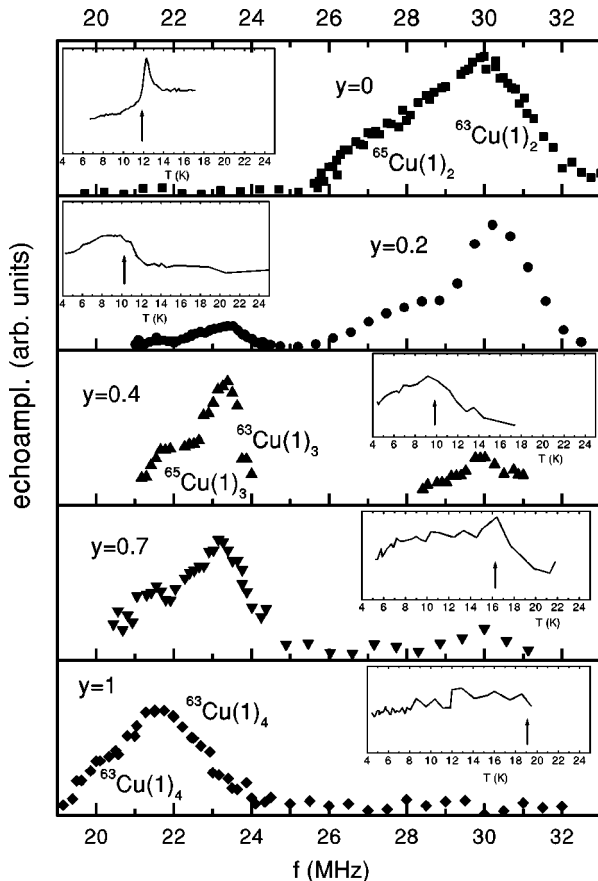
FIG. 3. Zero-field NQR spectra of the Cu(1) sites in Pr123. The assignment of the lines to the two-, three-, and fourfold oxygen coordination of Cu(1) corresponds directly to the one for the other RE123. The insets show the temperature corrected echo amplitude at constant excitation conditions versus temperature to illustrate the systematic change in the influence of the fluctuations at T_{N2} (arrows, see text).
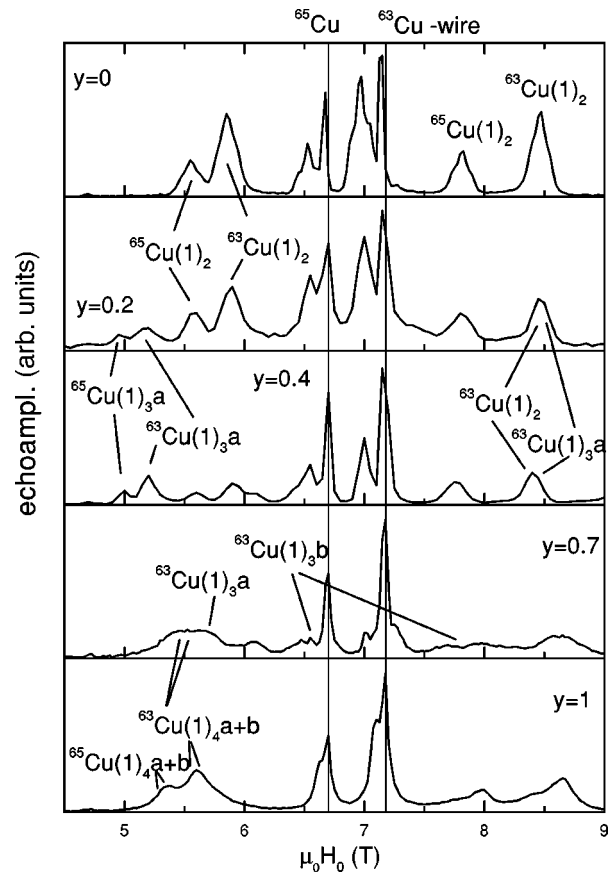
FIG. 4. Field-sweep spectra of the Cu(1) sites in Pr123 at 81 MHz and 4.2 K with the field along the (twinned) a and b axes. Together with similar spectra with the field along the c axis (not shown) the positions of the quadrupole satellite transitions determine the electric-field gradient tensor, their intensities the distribution of oxygen in the chains.

formation of (100)/(001) growth twins and, finally, even to (001)/(111) growth twins at large x. All orthorhombic crystals investigated in this work are twinned with respect to the a and b axes, but we find no indication for c-axis twins in the NMR spectra.

In Fig. 2 the low-temperature susceptibility in a field of 1 T perpendicular to the c axis clearly displays the cusp associated with the reorientation transition in the Cu(2) sublattice and the appearance of the Pr moments at various oxygen concentrations. The size and shape of the feature is very sensitive to sample quality and even depends on magnetic history of the sample.[80] In clean samples the transition temperature drops from near 17 K at $y=1$ to 12 K at $y=0$, similar to what we find in our crystals. The transitions occur at 14.9 and 12 K for the Ba-rich and the Pr-rich sample, respectively (not shown).

B. Cu(1)-O chains

Figure 3 shows the zero field spectra, Fig. 4 shows the field sweep spectra in Pr123 at various oxygen concentrations y. The spin-echo spectra were taken at 4.2 K and at comparably long pulse distances (≈ 40 μs) to suppress the contribution of the Cu(2) sites. The frequency range of

19–33 MHz for the NQR spectra of the Cu(1) sites in the antiferromagnetic RE123 (RE$\neq$Pr) and the assignment of the lines to the different oxygen coordinations of Cu(1) is by now well established.[35,34] The line positions and the relative intensities are similar to the ones observed in the other RE123, so we can safely use the same assignments [Cu(1)$_4$=21.8 MHz, Cu(1)$_3$=23.3 MHz, and Cu(1)$_2$ =30.1 MHz for ^{63}Cu]. The subscripts denote the number of oxygen in the Cu(1)-coordination shell, four for Cu(1) in a full chain, three for a chain end position, and two for the apex oxygen in an empty chain position.

The lines are significantly broader than in the other RE123 systems, where widths well below 100 kHz are observed in the homogeneous end members. The broadening may be due to structural defects inducing a distribution in the electric-field gradients (EFG), and to inhomogeneities in the magnetic structure of the Cu(2) lattice inducing inhomogeneous internal magnetic fields. The two cases can be distinguished from spectra obtained in a large external field, where the frequency of the central transition is to first-order independent of the EFG, so its linewidth is dominated by inhomogeneities of internal magnetic fields, while the distance between the satellites and the central transition is determined by the component of the EFG tensor along the magnetic field, so the satellites are broadened by both, distributions in

TABLE II. Comparison of the largest eigenvalue V_z (in 10^{-21} V/m^2), the asymmetry parameter η, and the eigenvalue of the EFG along the c axis, for the three Cu(1) coordinations in Y123 and Pr123.

Site	RE=Y			RE=Pr		
	V_z	$\|c$	η	V_z	$\|c$	η
Cu(1)$_2$	11.81	V_z	0.0	11.74	V_z	<0.05
Cu(1)$_3$	9.25	V_y	0.3	8.84	V_y	0.4
Cu(1)$_4$	8.4	V_x	>0.98	7.9	V_x	0.9($\pm$.1)

the EFG and in the internal magnetic field. In fact, both cases have been observed, Nehrke, Pieper, and Wolf found a significant narrowing of the Cu(1) lines above T_{N2} at $y=0$, a clear indication that magnetic disorder is present at low temperatures, while Grevin *et al.* confirmed our result that the magnetic transition at T_{N2} does not influence the linewidth at $y=1$, instead they find that the linewidth is due to the formation of a charge density wave at 100 K.[17,75]

The fluctuations at low temperature confirm, however, that the transition at T_{N2} in our crystals is magnetic.[17] The insets to Fig. 3 display the systematic change of this behavior with increasing oxygen content. The insets show the ^{63}Cu(1)-signal intensity, corrected for the Curie law of nuclear magnetization, versus temperature, measured across T_{N2} (arrows). The spin echo is measured at low temperatures with a repetition time shorter than the relaxation time T_1 for equilibration of the nuclear-spin system. Under such circumstances one expects that the amplitude increases when the relaxation time decreases, as is expected near a magnetic phase transition. The stoichiometric crystal at $y=0$ (top) clearly shows this behavior. T_1 decreases with increasing temperature and a pronounced minimum of T_1 at T_{N2} leads to a peak in signal intensity. With oxygen doping T_1 becomes shorter in the low-temperature phase, leading to a higher signal than above T_{N2}, and the relaxation induced peak at the transition is lost, presumably swamped by the large background of fluctuating fields in the ordered phase. At $y=1$ finally, no significant effects of the transition could be detected in this simple way. However, we found evidence for two contributions to the fluctuations in this temperature range for the fully oxidized crystal in full T_1 measurements. One component is almost independent of temperature and may be quadrupolar or magnetic, the other shows a broad minimum at T_{N2} and is ascribed therefore to magnetic fluctuations.[81]

The point symmetry of the Cu(1) sites implies that the principal axes of the EFG tensor for all oxygen coordinations are along the crystallographic axes. The full tensor is, thereby, determined by the assignment of the eigenvalues V_x, V_y, V_z (in ascending order of absolute values) to the axes, by the size of the largest eigenvalue V_z, and by the asymmetry parameter $\eta = |V_x - V_y|/V_z$. We determined these values from fits to the field-sweep spectra with the field along the c axis, and along the a and b axes. The values are compared in Table II with the ones observed in Y123. We cannot distinguish between the a and b axis in our twinned
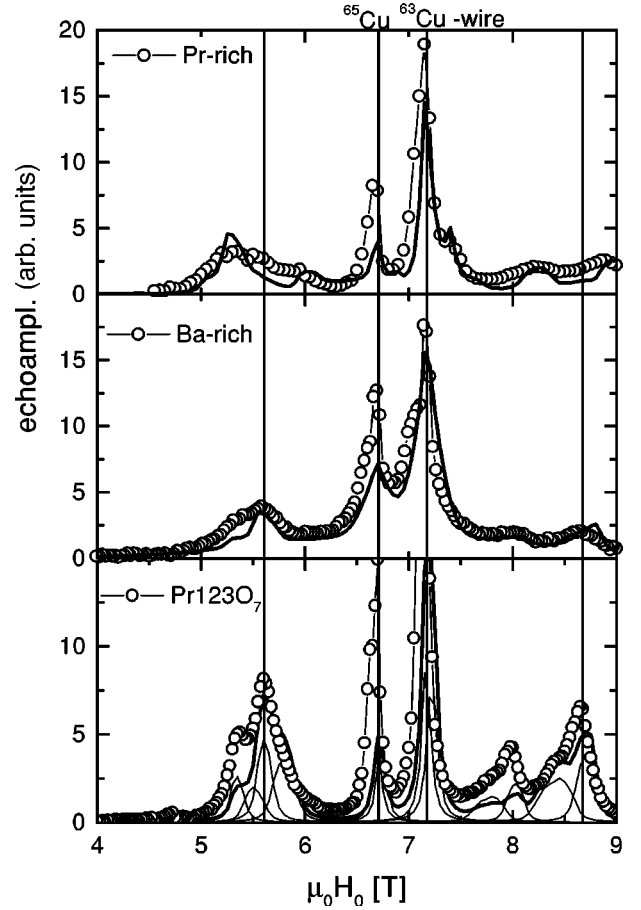

FIG. 5. Comparison of the field-sweep spectra of Cu(1) at 81 MHz in Pr123 at $y=1$ prepared in different oxygen atmospheres (see Table I). The vertical lines at the center transitions mark the Cu resonance from the wire of the pick-up coil, and at the ^{63}Cu satellites the position in the stoichiometric sample (bottom). The full lines are simulated spectra (see text for parameters). For the stoichiometric sample the decomposition into four subspectra (two isotopes in a field along the local x or y axis of the EFG) is also indicated.

crystals, therefore we give only the EFG component along c. The tetragonal symmetry of Cu(1)$_2$ implies $\eta=0$, as is observed.

In Fig. 5 we compare the field-sweep spin-echo Cu(1) spectra of the three fully oxidized crystals, again with the external field applied along the a and b axes. The fourfold coordination Cu(1)$_4$ characterized by the EFG tensor $\|V_{zz}\| \approx \|V_{yy}\|$ or $\eta \approx 0.9$ is the only one which we could identify in our crystals, as is expected for filled chains. All Cu(1) spectra are centered at the Cu resonance of the metal, showing that the Cu-chain sites detected in NMR carry no moment in these crystals. We emphasize that this means only that there is no homogeneous magnetization on the Cu(1) sublattice. Cu(1) moments localized at defect sites in the structure may well be undetectable by NMR due to short relaxation times.

The spectrum of the Pr-rich sample (top) shows a larger splitting than the stoichiometric one (bottom), an inhomogeneous broadening of the satellite lines, but no significant broadening of the central line. The high-field shoulder at 7.4 T of the ^{63}Cu-central transition can be assigned to the (111) growth twins mentioned above. As discussed above, the

broadening of only the satellite lines shows directly the presence of disorder in the charge distribution of the chain layer, clear evidence for the substitution of divalent Ba by tetravalent Pr and the disorder this defect site induces in the oxygen chains. On the other hand, the unchanged central linewidth proves the absence of internal magnetic fields at the Cu(1) site, indicating that the magnetic structure of the Cu(2) sublattice is not affected by the defects.

The spectrum of the nonstoichiometric Ba-rich crystal (center) is, in contrast, best described by two subspectra. One with approximately 30% relative intensity is the same as for the stoichiometric crystal, accordingly the environment of 1/3 of the Cu(1) sites is unchanged. A significant broadening of the central transitions together with a severe broadening of the satellites shows the presence of inhomogeneous magnetic fields together with charge disorder for the majority of the Cu(1) sites. The inhomogeneous width of the central transition corresponds to internal magnetic fields of ≈ 0.2 T, in full agreement with the transferred hyperfine fields from the Cu(2) moments at the Cu(1) site (≈ 0.1 T) that are known from studies of the so-called AF-II structure in Al-doped Y123.[55] The defects in this crystal do therefore introduce inhomogeneities in the magnetic structure of the Cu(2) sublattice.

The most plausible explanation for the fact that the size of the internal fields agrees well with the known transferred hyperfine field from the Cu(2) moments is that the divalent Ba dopes a hole state into the $d_{x^2-y^2}-2p\sigma$ band of the CuO$_2$ planes, similar to the well known case of Ca doping on the RE site in RE123. One might expect that this will form at low Ba concentrations in the RE sublattice a localized Zhang-Rice singlet, which in turn would lead to a Cu(2) moment missing in the configuration of the neighboring Cu(1) site. The intrinsic superconductivity of Pr123 crystals prepared under special conditions discussed recently is in view of these results most probably due to these holes becoming mobile at higher Ba concentrations, just as in the other high-T_c cuprates.

C. Pr resonance

We observed Pr resonances very similar to the ones reported in Ref. 18 in all crystals except one specimen with the nominal concentration $y=0$. In a second reduced crystal we found the signal, but its intensity is very small. Figure 6 shows the field sweep spectra at $y=0.2$, Fig. 7 shows the gyromagnetic lines for all samples. The signal is clearly due to ^{141}Pr since this is the only ion in the structure which may show van Vleck paramagnetism and the corresponding anisotropic enhanced gyromagnetic ratios γ_{eff} (the slopes at high fields, see below).

γ_{eff} is almost indendent of y, only for $y=0$ we find a higher value than in doped crystals with the field along the c axis, and a relatively small one with the field in plane. The fully oxidized, stoichiometric crystal is the only one where an orthorhombic distortion is detected by a splitting of the Pr-resonance line at low external in plane fields (see Ref. 18 for a detailed discussion of this effect). This does not prove, however, that the symmetry is tetragonal on a local scale for $y\lesssim 0.7$ in our crystals. A splitting similar to the one reported for $y=1$ might be hidden, because the smaller Pr signal at
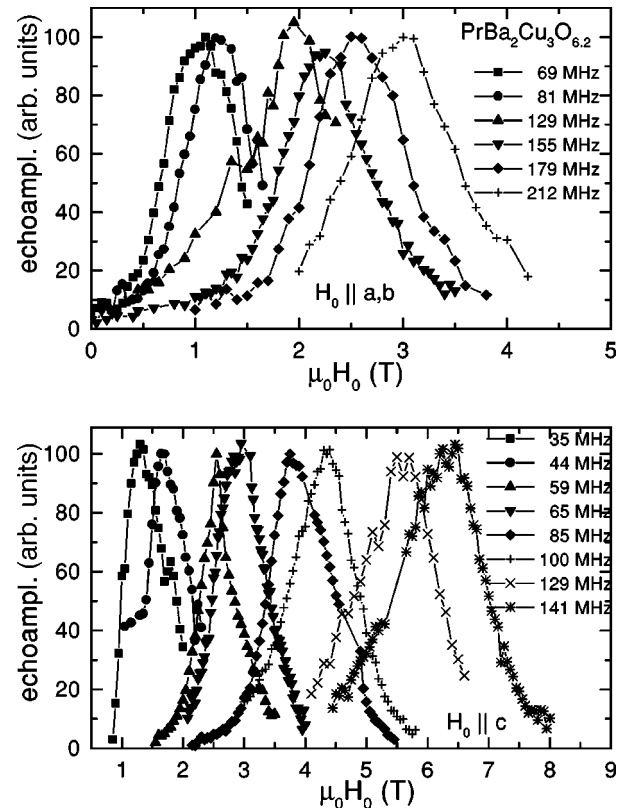

FIG. 6. Field-sweep spectra of Pr in slightly doped ($y=0.2$) Pr123 with the field along the c axis (top), and the a and b axis (bottom). At frequencies below ≈ 40 MHz there is increasing overlap with the Cu(1) spectra, especially Cu(1)$_2$ at small oxygen concentrations.

lower y overlaps with the very complicated Cu(1) spectrum. The linewidth is seen to be roughly proportional to the frequency or the optimum field, indicating that the inhomogeneous broadening is due to a distribution of the local gyromagnetic ratios with a width of approximately $\pm 10\%$. There is no indication of any unresolved quadrupole splitting like
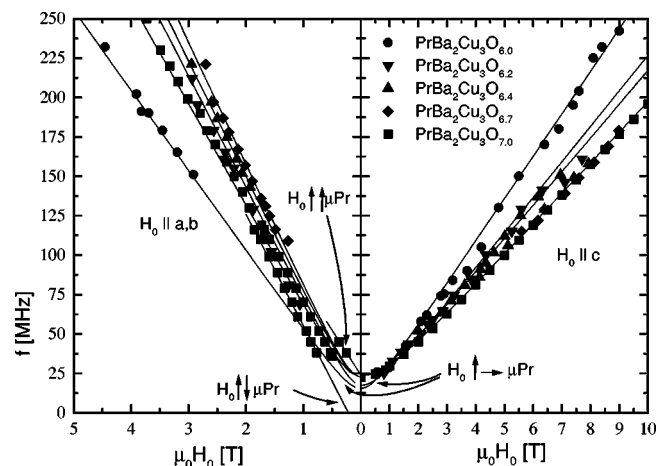

FIG. 7. Field dependence of the Pr-resonance frequency with the field applied along the c axis (right), and along the a and b axes (left) for the different oxygen concentrations y. The full lines were calculated for the van Vleck paramagnetism of the Pr-4f shell in the crystal field as described in the discussion. See Nehrke *et al.* for a detailed discussion of the line splitting in small in-plane fields.
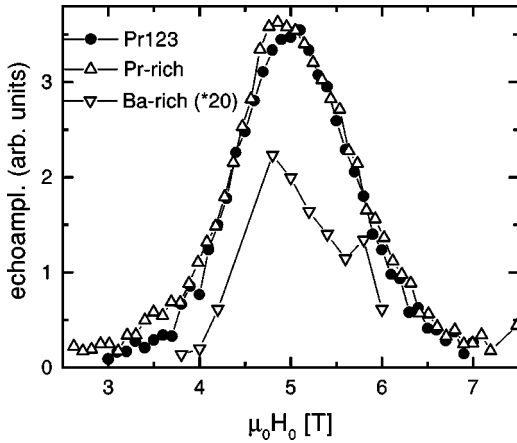
FIG. 8. Pr-field-sweep spectra at 102 MHz, 1.3 K, in a field $B_0 \| c$. The amplitudes are scaled to allow comparison of the line shapes. The signal in Pr123 is smaller by more than one order of magnitude.

the one observed in Pr_2CuO_4,[39] presumably because the EFG is even smaller at the nearly cubic Pr site in the Pr123 structure. We point out that the Pr linewidths turn out to be independent of oxygen content, in contrast to the Cu(1) resonances.

Comparison of the Pr spectra in the three fully oxidized crystals in Fig. 8 shows immediately that the effective gyromagnetic ratios and the linewidths of the stoichiometric and the Pr-rich sample are identical. The intensities of the two signals have been scaled to the same maximum for this comparison. The result shows most clearly that the local electronic state of the Pr ions contributing to the signal is the same in the stoichiometric and the Pr-rich crystal. As indicated above, there is no additional broadening in the Pr spectrum for off-stoichiometric oxygen concentrations, in contrast to the obvious inhomogeneous broadening of the Cu(1) resonance. This gives strong support to our earlier assignment of this signal to Pr on regular RE sites and not to the $[Pr]_{Ba}$ defect, because the regular site is shielded from the structural disorder in the chain layer by the CuO_2 planes.

In contrast to the similarities of the Pr resonance on the Pr-rich side of the solid solution system we have scarcely been able to detect any Pr resonance in the Ba-rich sample. Again this supports our assignment of the Pr signal, since Ba substituting for Pr introduces disorder in the RE sublattice and it has to be expected that large changes in the effective gyromagnetic ratios of the neighboring Pr sites will effectively wipe out the Pr signal from that region.

III. DISCUSSION

A. Hole doping

The hole doping mechanism of the CuO_2 planes with increasing oxygen content of the chains in the RE123 structure must be analyzed in two separate steps. First, the distribution of oxygen on the chain sites has to be determined, then the number of holes induced by the various Cu(1)-O configurations has to be found. Summation over the cluster probabilities times the corresponding hole counts should then yield the overall hole concentration for a given oxygen concentration y.[31] Cu(1) NQR may, in principle, contribute to both

questions. The resonance frequencies determine the quadrupole splittings and reflect the charge distribution, the relative intensities of the lines correspond to the probabilities of the different oxygen coordinations of Cu(1), so they give information on the oxygen distribution.

The EFG at Cu(1) sites depends sensitively on the charge distribution on the chains. It is hard to calculate the EFG in a correlated electron system from first principles, but for the chain layer local-density calculations show convincing results.[82] The main contributions arise from the charge distribution within the first Wigner-Seitz cell. This justifies the phenomenological ansatz to separate the EFG tensor into a contribution from the incompletely filled Cu-$d_{x^2-y^2}$ orbital and one from the p orbitals of the neighboring oxygens. Ohno, Koyama, and Yasuoka use for the Cu(1) site a $3d$ contribution of 117 MHz/hole and $n_{4p}\nu_Q^{4p} = -67$ MHz for the contribution from n_{4p} holes on the four oxygen neighbors,[38] making the quadrupole splitting very sensitive to the charge distribution in the chain layer. Nevertheless, from Table II the EFG of Cu(1) in Y123 and Pr123 is very similar for all oxygen coordinations. V_z in Pr123 is systematically smaller by $\approx 5\%$, which might well be due to the differences in the lattice constants, and η of $Cu(1)_4$ is somewhat reduced in Pr123, which might be connected to the relatively large defect concentrations. Furthermore, we found no evidence that the EFG at any of the Cu(1) coordinations depends on the oxygen content, in contrast to the expectations in case of a localization of the carriers in the 1D chains. We conclude that the results strongly support the ansatz that the substitution of Y by Pr has very little influence on the carrier concentration in the chain layer.

Cu(1) lines from sites in CuO clusters of different sizes are not resolved, so a direct determination of the cluster probabilities from the Cu(1) line intensities is not possible. Following the procedure described by Heinmaa et al.[34] we may estimate, however, the mean chain length $\langle n \rangle = 1 + 2I_4/I_3$ from the relative intesities I_4/I_3 of the three- and fourfold coordination. Note that there is no model for the oxygen distribution on the chain sites involved in this evaluation of $\langle n \rangle$. The small size of the crystals introduces a relatively large error in the orientation which has a strong influence on the field sweep spectra especially for $Cu(1)_3$. To check for consistency we compare the intensities with the concentration $y = I_3/2 + I_4$. If we consider only spectra which could be fitted consistently in this sense we arrive at the dependence of the chain length on y compared in Fig. 9 with the corresponding results from Lütgemeier et al.[35]

Systematic errors for $\langle n \rangle$ are due to the overlap of the broad lines and to the assumption that no Cu(1) contributions are missing in the experimental spectrum. It is quite possible that part of the Cu(1) sites cannot be detected in NMR, either due to very large line broadening from an inhomogeneous EFG distribution, or due to fast relaxation induced by slowly fluctuating on-site moments. As indicated above an ordered moment has been assigned to the chain sites in Pr123 by neutron diffraction. We can exclude the presence of a small moment homogeneously distributed over the whole Cu(1) sublattice. At $y \geq 0.4$ we find no evidence for magnetic line broadening, and for $y = 0$ the magnetic broadening of ≈ 0.2 T together with the Cu(2) hyperfine coupling constant in RE123 ($\approx 13.4 T/\mu_B$) sets an upper limit of $0.02\mu_B/Cu$
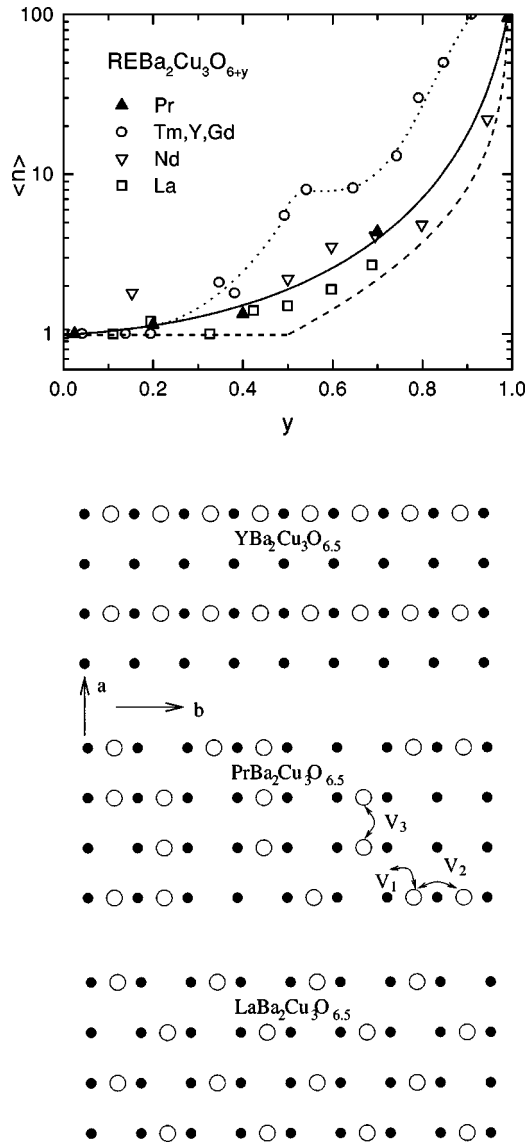
FIG. 9. Comparison of the mean Cu(1)-O-chain length versus y determined from the relative intensities of the Cu(1) lines in RE123 with RE=La, Tm, Gd, Nd, Y (Ref. 35), and Pr (this work). The full line sketches the expected behavior for a random distribution of chain oxygen, the dashed for repulsive O-O interaction V_2, and the dotted for attractive V_2. The bottom part shows the corresponding distributions of oxygen on the chains at half filling. This dependence of the oxygen distribution on the RE radius may lead to a smaller doping of the CuO$_2$ layer at intermediate y for larger RE, but the influence of the RE radius on $T_{cmax} = 89$–96 K is only small.

for the crystals with low oxygen concentrations. However, we cannot exclude the existence of localized moments on Cu(1)-sites neighboring defects. We emphasize again that such defect induced moments determine most probably the low-temperature magnetism of the Cu(2) sublattice in Al-doped samples,[83] and they might well be present on Cu(1) neighbors of Pr on Ba sites.

Despite this uncertainty in the integrated intensity of the Cu(1) spectrum, which is common to some extent to all RE123 compounds with light RE, our experimental chain lengths compare favorably with the expectation for the chain length in the asymmetric next-nearest-neighbor Ising (ASYNNNI) model with vanishing V_2, the interaction of two oxygen nearest neighbors with Cu(1) in between (see bottom of Fig. 9). The large, repulsive interaction V_1 drives the formation of chains with diverging length at $y = 1$ in the ortho-I structure. The formation of the ortho-II superstructure of alternating empty and long chains in Y123 at $y = 0.5$ is due to an attractive V_2 in the case of a small RE. If V_2 is strongly repulsive the so-called herringbone superstructure is stable at $y = 0.5$, and $\langle n \rangle$ will be one up to that point. This case is apparently nearly realized with the large La ion on the RE site. Nd with a radius in between is well described by a random distribution of the oxygen on chains, as is Pr. The origin of this influence of the RE ion on the interaction potential of oxygen in the ASYNNNI model is not clear at this time, but Pr123 fits smoothly into the trend. This finding underlines the conclusion above that Pr has no extraordinary influence on the electronic state of the Cu(1)O clusters.

The concentration of hole states in the CuO$_2$-Pr-CuO$_2$ trilayer should then be at all oxygen concentrations similar to the one in Y123, namely below the ≈ 0.35/unit cell in (superconducting) Y123 at $y = 1$. Cluster and band-structure calculations of the chemical potential as a function of the chain length in Y123 indicate that only clusters of a length above approximately three oxygen sites can induce hole states in the CuO$_2$ planes.[36] Therefore the reduced average chain length in Pr123 may lead to a somewhat smaller hole concentration in Pr123 than in Y123 at the same y, at least if this threshold behavior occurs in Pr123 as well. Besides this small difference we arrive at the conclusion that on average at most every third Pr localizes a hole within the CuO$_2$-Pr-CuO$_2$ planes of the structure.

B. Pr-4f ground state

From the above arguments we are convinced that we can use the Pr resonance to probe the charge distribution in the CuO$_2$-Pr-CuO$_2$ trilayer by its effect on the crystalline electric field (CEF) of the Pr-4f shell. In cases where the NMR signal of non-Kramers ions like trivalent Tm or Pr can be observed, rather detailed information especially on the low-energy part of the CEF Hamiltonian is obtained.[39] An experimental determination of the crystal field at Pr from NMR is the more desirable since the spectra obtained in Pr123 by INS are heavily broadened and the difficulties in their analysis lead to a considerable scatter in the CEF-energy level schemes.[15] A more extensive description of our analysis of the crystal-field Hamiltonian $\mathcal{H}_{cf}$ than was possible in Ref. 18 seems to be in order in view of the controversal discussion initiated by the results obtained for the crystal with the highest oxygen concentration.

As stated above, the anisotropic enhancement of the gyromagnetic ratio ($^{141}\gamma = 13$ MHz/T without van Vleck contributions) unambiguously identifies the signal as due to ^{141}Pr. It is, however, more difficult to identify the position of the Pr in the lattice, and it has been argued that our NMR experiments might detect the signal from the $[Pr]_{Ba}$-defect sites.

There is strong experimental evidence against the assignment to the defects. As indicated above, the linewidth of the Pr resonance is independent of any oxygen- or Ba-site disorder in the chains, though this is clearly reflected in the Cu(1)
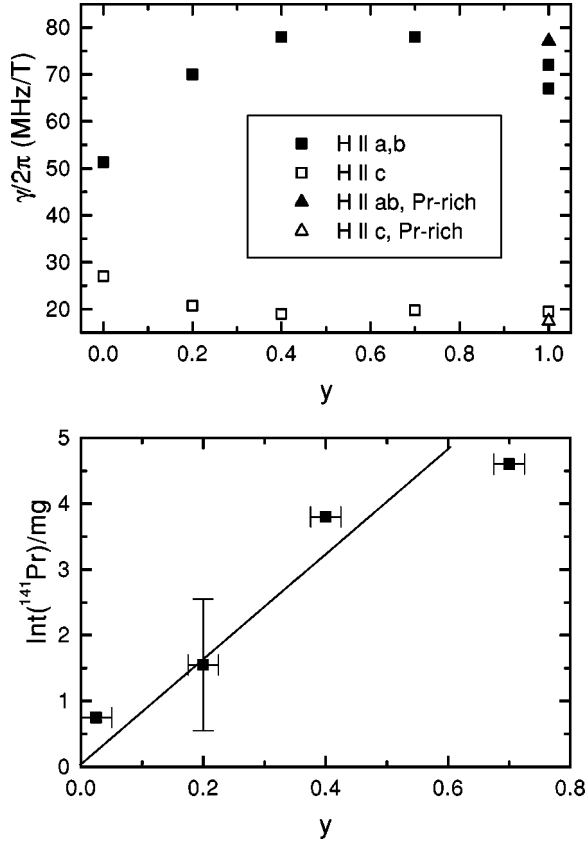
FIG. 10. Dependence of the effective gyromagnetic ratios of Pr (top), and the Pr signal amplitude normalized to sample volume (bottom) on the oxygen concentration. The error bars in the right figure indicate along y the uncertainty from the relative Cu(1)-line intensities, along the intensity axis they estimate the uncertainty due to the different filling factors of the NMR coils. The sample denoted throughout the text by $y=0$ for convenience is almost certainly not fully reduced. In a second crystal with the same Cu(1) spectra we observed no Pr resonance at all.

spectra at intermediate y or off-stoichiometric Pr/Ba cation ratio. Second, Figs. 7 and 10 show in accord with the detailed crystal-field analysis below that the van Vleck susceptibility tensor is very nearly tetragonal, and almost independent of y. This shows a tetragonal symmetry of the CEF, independent of the oxygen contents of the chains. A symmetry close to tetragonal is in full accord with the expectation for the regular Pr site at all y, because the site is far from the chain layer and shielded by the CuO_2 planes. The CEF of Pr on Ba sites, on the other hand, is expected to reflect the orthorhombic symmetry at $y=1$, where the neighboring chains are filled, but also at small y, because Pr^{3+} is known to bind oxygen on the neighboring O(5) sites. In addition, Allenspach *et al.* showed that the CEF of $[Nd]_{Ba}$ is completely different from the one on the RE site,[84] while we show below that the CEF we find from our results and the one determined from INS are rather similar. The strong asymmetry of this configuration has been observed in the EFG of La on the Ba site.[85]

The connection between the anisotropic γ_{eff} observed in Fig. 7 and the CEF can be understood in terms of a single-ion description of the $4f$ shell. In Ref. 18 we derive the nuclear spin Hamiltonian

$$\mathcal{H}=\left(\hbar\gamma+\frac{A_J}{g_J\mu_B}\chi_\alpha\right)I_\alpha\mu_0H_{0,\alpha}+\frac{A_J}{g_J\mu_B}\langle M_\alpha\rangle_{sp}I_\alpha$$

$$=\hbar\gamma_\alpha\mu_0H_{0,\alpha}I_\alpha+\frac{A_J}{g_J\mu_B}\langle M_\alpha\rangle_{sp}I_\alpha \quad (3.1)$$

for the nuclear spin $\mathbf{I}$ coupling with a gyromagnetic constant $\gamma/2\pi=13.0$ MHz/T to the external field H_0, and via the hyperfine coupling constant $A_J/h=1093$ MHz to the moment $\langle\mathbf{M}\rangle$ in a $4f$ shell with angular momentum J and Lande factor $g_J=0.8$. $\chi_\alpha=\partial M_\alpha/\partial H_\alpha$ is the static van Vleck susceptibility with the field along the crystallographic axis $\alpha=a,b,c$, $\langle M_\alpha\rangle_{sp}$ is the spontaneous Pr moment along one axis. The diagonalization of $\mathcal{H}$ for $H_0\|\mathbf{M}_{sp}$ or in the case of large external fields is trivial in the notation with the effective gyromagnetic ratio γ_α in the second part of Eq. (3.1). The gyromagnetic ratio γ changes to

$$\gamma_\alpha=\gamma+\frac{A_J}{\hbar g_J\mu_B}\chi_\alpha, \quad (3.2)$$

which is independent of temperature and field as long as this is the case for the van Vleck susceptibility. This holds for temperatures and fields $k_BT,\mu_0H_0\langle M\rangle_\alpha\ll\Delta_\alpha$, where Δ_α is the smallest CEF splitting of $4f$ levels connected by J_α. From the linear field dependence of the resonance frequency in Fig. 7 it is clear that γ_α at 1.3 K is indeed independent of the field up to at least 9 T (5 T for the field in the plane). The offset and the slope of the gyromagnetic lines determine immediately the spontaneous Pr moment $\langle M\rangle_{sp}$ and the local susceptibility χ_α, respectively.

The frequency offset is clearly smaller than 25 MHz for all samples. It corresponds to a very small ordered moment of below $h\nu/A_J=0.023\mu_B/Pr$ in all cases, more than one order of magnitude smaller than the $0.3-1.2\mu_B$ detected with neutron diffraction or Mössbauer spectroscopy. It was perhaps this property which gave rise to the most severe doubts about the interpretation of our spectra of the fully oxidized sample.

In order to understand the origin of this discrepancy it is usefull to discuss first the CEF. We compare the three experimental components of χ_α,

$$\chi_\alpha=\frac{\hbar g_J\mu_B}{A_J}(\gamma_\alpha-\gamma), \quad (3.3)$$

with the ones calculated in the eigenbasis of a suitably modelled crystal-field Hamiltonian $\mathcal{H}_{cf}$ ($\mathcal{H}_{cf}|k\rangle=\varepsilon_k|k\rangle$):

$$\chi_\alpha=(g_J\mu_B)^2\sum_k\left[\frac{1}{k_BT}\sum_l^{\varepsilon_l=\varepsilon_k}|\langle k|J_\alpha|l\rangle|^2e^{-\varepsilon_k/k_BT}\right.$$
$$\left.+\sum_l^{\varepsilon_l\neq\varepsilon_k}|\langle k|J_\alpha|l\rangle|^2\frac{e^{-\varepsilon_k/k_BT}-e^{-\varepsilon_l/k_BT}}{\varepsilon_l-\varepsilon_k}\right]. \quad (3.4)$$

Because of the exponential factors in Eq. (3.4) the susceptibility is dominated by the matrix element of the total angular momentum with the ground state and the lowest excited state with nonvanishing matrix element. The most conve-

nient representation of $\mathcal{H}_{cf}$ for a calculation of χ_α is by means of the Stevens equivalent operators $\mathcal{O}_l^m$ with crystal-field parameters b_{lm}:

$$\mathcal{H}_{cf} = \sum_{lm} b_{lm} \mathcal{O}_l^m . \qquad (3.5)$$

It describes the two $4f$ electrons in Russel-Saunders coupling. The LS admixture from spin-orbit coupling,[86] which is 3100 K,[87] and the interconfiguration coupling, i.e., the admixture of states from the multiplets $J=5,6$ considered by Hilscher *et al.*,[15] are neglected. This may be justified as a first approximation since the spin-orbit coupling is significantly larger than the crystal-field splitting. Then $\mathbf{J}=\mathbf{L}+\mathbf{S}$ is a good quantum number and the ground state of an isolated Pr^{3+} is the ninefold $^3H_4$ multiplet, which is further split by $\mathcal{H}_{cf}$, or by a magnetic field. The representation is based on the Wigner-Eckhard theorem, which guarantees that the matrix elements of $\mathcal{H}_{cf}$, taken within a subspace of states $|LSJM_J\rangle$ with fixed quantum numbers L, S, and J, are proportional to a suitable polynomial $\mathcal{O}_l^m$ of angular momentum operators. The equivalent operators and the numerical factors occurring in the Wigner-Eckard theorem are tabulated by Hutchings.[88]

The advantage of the equivalent operators $\mathcal{O}_l^m$ is that the matrix elements can be calculated in a physically transparent way, since they contain only angular momentum operators, and usually a good fit of the energy spectrum is possible. We follow therefore the common practice in NMR and use below equivalent operators. Note that A_J and g_J enter both experimental parameters, the slope and the offset of the gyromagnetic lines. The values for A_J and g_J introduced above are the ones for the $^3H_4$ multiplet, and they allow for a fit to the gyromagnetic lines with reasonable parameters. This is not possible if A_J is chosen significantly higher (to allow for a higher $\mathbf{M}_{sp}$), because then unphysically large moments result in high field.

A good fit of the CEF energy spectrum from within the $J=4$ multiplet alone does, however, not necessarily imply the same precision for the crystal-field parameters. The analysis of the INS spectra is usually based on a irreducible representation of $\mathcal{H}_{cf}$ by spherical harmonics and shows admixture of states from higher configurations. The conversion factors for the crystal-field parameters B_{lm} used in the irreducible representations and the b_{lm} above may be determined by comparison of the coefficients with equal symmetry and have been tabulated by Kassman.[89] A comparison of $\mathcal{H}_{cf}$ in the two representations is difficult if the interconfiguration mixing has significant influence. In this case differences may occur in the eigenvalues of $\mathcal{H}_{cf}$ calculated from the irreducible representation and the ones calculated from the equivalent operator representation after conversion of the parameters.

For $4f$ electrons spherical harmonics up to the order $l = 2 \times 3 = 6$ and $m \leq l$ can contribute to the series in Eq. (3.5). The point symmetry of Pr allows only for even l ($=0,2,4,6$) and $m(=0,2,4,6\leq l)$ in orthorhombic point symmetry, and the fourfold c axis in tetragonal symmetry reduces this further to $l=2,4,6$ and $m=0,4\leq l$. Obviously it is impossible to determine the full set from the three compo-

nents of the local susceptibility χ_α, and in Pr123 even the more detailed information from INS is insufficient. Fortunately, both methods are complementary: NMR is sensitive to the ground-state symmetry and the splitting of only the low-lying levels, while the INS spectra suffer especially at low energy from the severe broadening, but well resolved lines are observed ≈ 500 K above the ground state.

A simultaneous fit of $\mathcal{H}_{cf}$ to the results of both methods is viable only for the samples with high oxygen concentrations y. The difficulty is that our ground-state symmetry for all y must be tetragonal with at most a very small orthorhombic distortion. The severe line broadening of the INS spectra does not allow us to determine the ground-state symmetry unambiguously for $y=1$, but for $y=0$ any description with tetragonal symmetry is very poor. We have therefore apparently conflicting results from the two methods at $y=0$.

In order to solve the problem we propose to take the results of both experiments at face value and assume the presence of Pr in two different symmetries on the RE sites. We emphasize that the presence of two distinguishable electronic configurations of Pr was already proposed by Fehrenbacher and Rice, so we use below their nomenclature for the two sites. Here we only make use of the fact that the CEF should be different for Pr^{3+}, the site without a hole state in its $4f$ shell and in the $2p\pi$ orbitals of the eight oxygen ligands, and for Pr^{IV}, the site where a hole is localized in the $4f$ shell and the $2p\pi$-ligand orbitals. The concentration of the Pr^{IV} configuration is according to Fehrenbacher and Rice directly the hole concentration n_h determined above from the Cu(1) resonance, that is at most ≈ 0.35 holes per unit cell or roughly every third Pr site.

First we assign the Pr resonance detected in NMR to the Fehrenbacher-Rice state Pr^{IV}, and Pr^{3+} to the signal obtained in INS (and most other techniques). From the NMR point of view this is natural because the intensity of Pr resonance increases with y, that is, with the number of holes (see Fig. 10). From the INS results the assignment is necessary because a signal is present at $y=0$ and the CEF observed is at all y similar to the one determined with very high accuracy for other RE in RE123, where the hybridization state Re^{IV} does not exist.

The contradicting results of INS and NMR for the reduced samples ($y=0$) are now easy to understand. NMR observes a small signal from a few percent of Pr in the state Pr^{IV}, which may be induced, e.g., by a small amount of oxygen remaining on chain sites. In INS the small signal corresponding to these sites is probably not detected. On the other hand, the Pr resonance from the state Pr^{3+} dominating the INS spectra may well be not observable in NMR, either due to fast relaxation, or due to a large inhomogeneous broadening from the EFG of the distorted $4f$ shell and the magnetic hyperfine fields induced by $4f$ moments.

Near $y=1$, where approximately 1/3 of Pr is expected to be in the state Pr^{IV}, they certainly contribute to the INS spectra. Then we must seek for a simultaneous fit of $\mathcal{H}_{cf}$ to the NMR data and the INS spectra, weighted for their high sensitivity at low and high energies in the spectrum of $\mathcal{H}_{cf}$, respectively. Any differences in the CEF energies of the two Pr configurations must be compatible with the supposedly inhomogeneous linewidth of the INS spectra at energies above approximately 500 K.
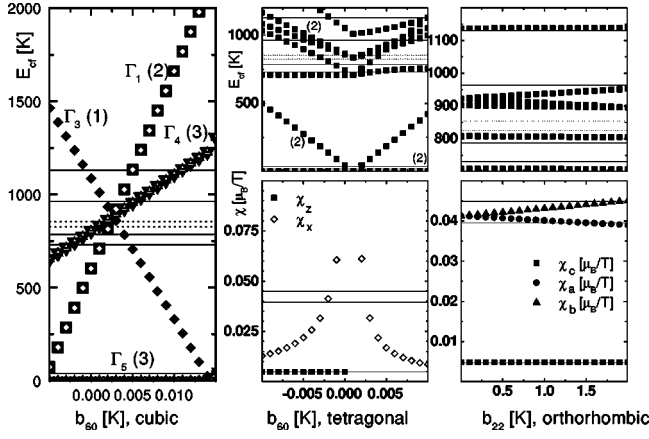
FIG. 11. Determination of the crystal-field parameters b_{lm} by successively lowering the symmetry in the fit from cubic (left), to tetragonal (center), to orthorhombic (right). The horizontal lines represent the crystal-field splittings determined by INS (left and top figures) and the van Vleck moments of Pr determined from our NMR data (bottom figures). Note that the upper-right figure contains only the levels at high energies, showing that a reasonable fit to the energies in the resolved part of the INS spectra is achieved with this simple procedure.

The method we use to fit of $\mathcal{H}_{cf}$ to the NMR data and the high-energy part of the INS spectrum is motivated by the almost cubic oxygen coordination of the RE site in RE123. We start from a CEF with cubic symmetry. We then improve this solution with a tetragonal distortion, which we may "polish up" with an additional orthorhombic distortion and a local magnetic field.

The three steps are shown in Fig. 11. There is a general consensus from all experimental techniques that the cubic Γ^5 triplet is the subspace underlying the quasitriplet at low energies of $\mathcal{H}_{cf}$ in Pr123. We therefore adjust the two parameters b_{40}, b_{60} of the cubic $\mathcal{H}_{cf}$ (see Ref. 90) to fit the splitting between the ground state and the other levels, and the one between the other levels roughly to the experimental energies from INS. The left panel shows the regime of b_{60} for cubic symmetry, where the Γ_5 triplet is the ground state (b_{40} is fixed at 0.335 K). We choose $b_{60} = 0.001$ K as a cubic approximation.

Next we consider a tetragonal distortion by variation of b_{60} with $b_{64} = -0.021$ K fixed at its cubic value (center panels). The Γ^5 triplet splits into a doublet and a singlet, which are the ground state for b_{60} larger or smaller than the cubic value, respectively (top part). The local susceptibility (bottom part) χ_z fits the local susceptibility observed in the NMR experiment (horizontal lines) only if the singlet is the ground state. χ_z is too large by two orders of magnitude if b_{60} is larger than its cubic value (in the right half of the central panels). With the singlet ground state the tetragonal χ_x ($\diamond$) falls between the orthorhombic in-plane susceptibilities at $b_{60} = -0.002$ K. Simultaneously the splitting of the upper levels is described more or less correctly (top). At small y, where we find tetragonal symmetry, this procedure leads to the parameters given in Table III.

The crystal $y = 1$ is the only one where we found an orthorhombic splitting, and here we introduce the orthorhombic distortion b_{22} shown in the right panel of Fig. 11. The changes in the high-energy eigenvalues are small (top, note the suppressed zero), and even the eigenvectors of $\mathcal{H}_{cf}$ change only by a few percent. The fit to the transitions observed in INS (horizontal lines) is already reasonable. The local susceptibilities (bottom) are well described at $b_{22} = 1.9$ K. We may now use the other parameters to "polish the fit up," but we emphasize that this is far from unambiguous and any improvement is probably beyond the accuracy of the description with Stevens equivalent operators. The parameters given for $y = 1$ in Table III are an example for an almost exact fit to the local susceptibility *and* the energies above 500 K.

Figure 12 shows a polar diagram of the charge distribution in the two-electron ground states calculated from our crystal-field parameters for $y = 1$, and from the converted crystal-field parameters of Hilscher *et al.*[15] The state Pr^{IV} observed in NMR is tetragonal, the small orthorhombic distortion is not visible. The eight lobes pointing along the space diagonals of (nearly) a cube with oxygen at the corners resemble closely the $4f$ state envisaged by Fehrenbacher and Rice.[22] Note that there are four additional lobes in the plane perpendicular to the c axis pointing to the edges of the cube. The ground state Pr^{3+} observed in INS looks very different at first sight, but from the above discussion the connection

TABLE III. Top: Crystal-field parameters determined from the simultaneous fit to the high-energy INS spectra and to the local susceptibilities measured by NMR in the case of Pr123, $x = 1$. Since we find tetragonal symmetry for the local susceptibility we fit only to χ_α for Pr123, $y = 0$, and searched for the nearest solution in the parameter space to the one of $y = 1$. Bottom: Eigenvalues of $\mathcal{H}_{cf}$ as determined by Hilscher *et al.* from INS (Ref. 15), and from our NMR data. Values in brackets are not directly observed. Note that we did not intend to fit the energies in the case $y = 0$.

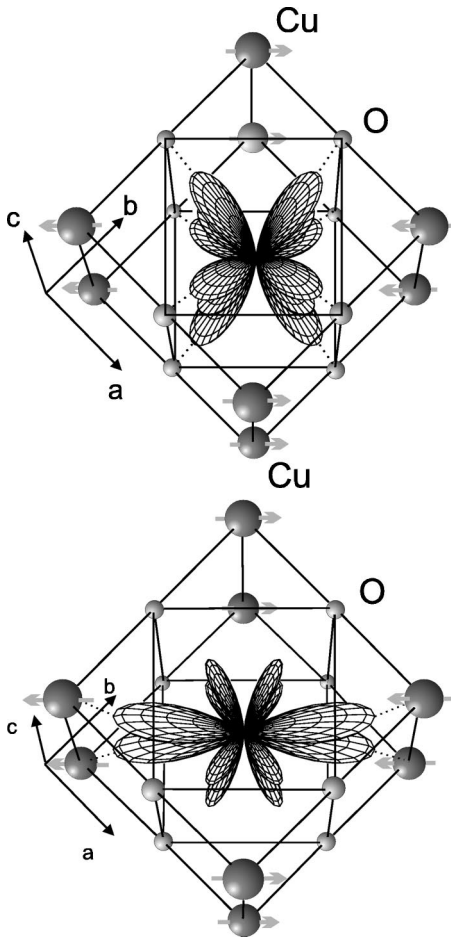| b_{lm} [K]	b_{20}	b_{22}	b_{40}	b_{42}	b_{44}	b_{60}	b_{62}	b_{64}	b_{66}
$y = 1$	-1.9	1.2	0.325	0	1.665	-0.0022	0	-0.0252	0
$y = 0$	0	0	0.335	0	1.675	-0.0069	0	0.05	0
$E_{cf}(y=1)$									
INS [K]	0	17	38	731	786	(825)	(854)	963	1130
NMR [K]	0	132	142	726	(775)	(832)	(922)	(956)	(1126)
$E_{cf}(y=0)$									
INS [K]	0	20	39	714	(727)	(733)	757	882	983
NMR [K]	0	208	208	351	(506)	(835)	(866)	(866)	(1452)

FIG. 12. Polar plot of the shape of the $4f^2$ wave function of Pr as determined from our NMR data (top), and from INS (bottom). The (tetragonal) c axis points to the top, the eight lobes along the local (111) directions point to the oxygen neighbors. Only one of the two possible orthorhombic ground states for INS is shown, the other one is rotated by $\pi/2$ around the c axis.

between both states is easy to visualize: Rotations of Pr^{IV} by 90° around the local x or y axis ($\perp c$) lead to the two remaining states of the cubic Γ^5 triplet, the doublet in the tetragonal symmetry. In a suitable orientation of the local x and y axes such a rotated Pr^{IV} state resembles closely the state Pr^{3+} in the figure, only the four lobes which were formerly perpendicular to c are more pronounced. Note that the orientation of the local x and y axes or these four dominant lobes is determined only when, e.g., a Jahn-Teller distortion lifts the twofold degeneracy of this ground state in tetragonal symmetry.

The physical origin for the different ground-state symmetries is in our model the one missing electron charge in the $2p\pi$-ligand orbitals of the oxygen coordination of Pr in the state Pr^{IV}. In the presence of this hole the tetragonal CEF is on the left-hand side in Fig. 11 with the singlet ground state. If the orbitals are occupied the CEF changes to the right-hand side and the doublet becomes the ground state. The doublet degeneracy may be lifted by a Jahn-Teller distortion leading to the ground state observed by INS.

C. Low-temperature magnetic structure

We now turn to the low temperature magnetic state of Pr. All crystals investigated here show the well-known kink in the low-temperature susceptibility, indicating a magnetic transition at temperatures increasing with oxygen content from ≈ 10 to 18 K (see Fig. 2). In the discussion following our first observation of nonmagnetic Pr it became clear that there is a simultaneous transition in the magnetic structure of the Cu(2) sublattice, but even taking this complication into account moments of at least $0.5\mu_B$/Pr are required to describe the magnetic Bragg peaks at all y.

The observation of a Pr moment is consistent with the interpretation presented above if the state Pr^{3+} carries this moment, and the existence of two magnetically different sites has been considered much earlier as a possible explanation for the broad [141]Pr-Mössbauer spectra.[79] The fact that T_N *increases* with the concentration of the *nonmagnetic* site Pr^{IV} is, however, in clear contradiction to the concept that Pr-Pr exchange is the origin of the transition. Even the fact that the transition occurs at all would be surprising at $y=1$, because the magnetism of the RE sublattice is known to be strongly two dimensional, and the percolation threshold for the square lattice with nearest-neighbor exchange is only 0.5928. The 30% nonmagnetic impurities introduced by hole doping would bring the lattice almost to the percolation. Obviously a similar difficulty with the exchange coupling arises with the small dependence of the Pr T_N on magnetic dilution by other RE ions.

We propose therefore that the Pr moments are induced by the transition in the Cu(2) sublattice. The mechanism is the same we introduced in our previous work,[18] but now we have to consider two different Pr sites. The different magnetic properties of the two Pr sites are a direct consequence of the two ground-state symmetries discussed above: The tetragonal symmetry of the state Pr^{IV} has as a consequence the cancellation of all transferred hyperfine fields from Cu(2) at the Pr site, therefore the Pr moment vanishes. The small moment indicated by the offset in the resonance frequency may be induced by dipolar fields from the Cu(2) moments, which do not fully cancel by symmetry.

On the other hand, the four pronounced lobes of the state Pr^{3+} can point to the center of the edges of the cube spanned by the oxygen, that is, to four of the Cu(2) sites (see Fig. 12). Note that these moments are parallel in the structure proposed as a first approximation in Ref. 18 and sketched in the figure, and that they do have a parallel component in the refined structure determined later by neutron diffraction. In such a case the transferred hyperfine fields at the Pr site do not cancel. The size of the induced moments depends exponentially on the small splitting of the quasitriplet in the CEF [see Eq. (3.4)]. Despite the considerable scatter in the CEF parameters determined for Pr^{3+} from INS it is clear that the splitting is smaller by at least a factor of 2 than the 130 K we obtained above for the state Pr^{IV}, with the result that a transferred hyperfine field in the order of 1 T can be sufficient to induce the observed moments.

Note that no extraordinarily high Pr-Pr exchange is required to explain the surprisingly high T_N in this model, therefore the problem of the small dependence of the transition temperature on magnetic dilution does not occur. However, an exchange interaction of the order of 1 K may help to understand at least qualitatively the peculiar orientation of the Pr moments, halfway between the CuO$_2$ plane and the c axis.[91,41] If the Pr moments are induced by internal fields

rather than due to $4f$-$4f$ exchange interactions the magnetic structure of the Pr sublattice is expected to reflect the one of the Cu(2) sublattice, a feature which might be used to check our model. In this context it is interesting to note that Pr orders magnetically at exceptionally high T_N in a number of related cuprates when it is situated between antiferromagnetic (insulating) CuO_2 sheets.[45–47] To our knowledge, there has been only one report of coexistence of Pr order and superconductivity,[92] but the sample was inhomogeneous and only partially superconducting, so magnetic order and superconductivity might be located in different volume fractions.

IV. CONCLUSIONS

We reported NMR/NQR investigations of the charge distribution in $Pr_{1+x}Ba_{2-x}Cu_3O_{6+y}$ crystals at low temperature. Comparison of the EFG at Cu(1) in the chains with the one in Y123 confirms the assumption of the hybridization model, that the hole states doped with increasing y into the structure are not localized in the chain layer but in the CuO_2-Pr-CuO_2 trilayer. The relative intensities of the resonances corresponding to the different oxygen coordinations of Cu(1) in the chains show that there is no tendency to form O-Cu(1)-O chains with Pr on the RE site, a result which fits nicely into the trend of the interaction of oxygen on chain sites with the RE radius.

Our investigations of the Cu(1) and Pr resonance in off-stoichiometric crystals in the Pr/Ba solid solution system show that the accessible concentration range for x in $Pr_{1+x}Ba_{2-x}Cu_3O_{6+y}$ can be extended to negative x by preparation at reduced partial oxygen pressure. The fingerprint of the $[Ba]_{Pr}$ defect in the Ba-rich crystal is a wipeout of the Pr-signal and an inhomogeneous internal magnetic field at the Cu(1)-site, which we ascribe to localized singlet states in the antiferromagnetic CuO_2 layers. $[Pr]_{Ba}$ in the Pr-rich crystal, on the other hand, does not influence the Pr resonance or induce disorder in the magnetic Cu(2) structure, but the structural and charge disorder in the chain layer is evident from the inhomogeneity of the Cu(1)-quadrupole splittings. These findings give strong support to our earlier assignment of the Pr signal to regular (RE) sites.

The Pr resonance was observed in all crystals except one fully reduced, stoichiometric specimen. In order to give a consistent interpretation of this NMR signal as well as for the observations from INS and the volume probes, we propose that the two electronic Pr configurations introduced by Fehrenbacher and Rice correspond to two different ground-state symmetries of Pr in the RE layer. We provide evidence that NMR detects only the state with a hole localized in its $4f$ shell and the $2p\pi$ orbitals of the surrounding oxygen ligands, while the properties observed with space-integral techniques like INS are dominated by the response from sites without such a localized hole. The model is supported by our count of localized carriers with the Cu(1) resonance, the decreasing intensity of the Pr resonance with decreasing oxygen concentration y, by our detailed analysis of the CEF of Pr, and it explains the discrepancy in the magnetic states of Pr observed in NMR on one hand, and INS and susceptibility on the other. Finally, we argue against the assumption of a strong, enhanced $4f$-$4f$ exchange as the origin of the extraordinarily high Pr ordering temperature and the suppression of superconductivity. As an alternative we propose that the Pr moments are induced by internal fields which appear due to the reorientation transition of the Cu(2)-moments.

*Electronic address: Pieper@xphys.tuwien.ac.at

[1] H. B. Radousky, J. Mater. Res. **7**, 1917 (1992).

[2] S. Hüfner, Adv. Phys. **43**, 183 (1994).

[3] W. E. Pickett, Physica C **289**, 51 (1997).

[4] J. L. Tallon, C. Bernhard, H. Shaked, R. L. Hitterman, and J. D. Jorgensen, Phys. Rev. B **51**, 12 911 (1995).

[5] H. Zhang and H. Sato, Phys. Rev. Lett. **70**, 1697 (1993).

[6] J. J. Neumeier and M. B. Maple, Physica C **191**, 158 (1992).

[7] G. Cao, Y. Yu, and Z. Jiao, Physica C **301**, 294 (1998).

[8] S. Skanthakumar, J. W. Lynn, N. Rosov, G. Cao, and J. E. Crow, Phys. Rev. B **55**, R3406 (1997).

[9] Z. Tomkowicz, Physica C **320**, 173 (1999).

[10] I. Francois, C. Jaeckel, G. Kyas, D. Dierickx, O. van der Biest, R. M. Heeres, V. V. Moshchalkov, Y. Bruynseraede, H. G. Roskos, G. Borghs, and H. Kurz, Phys. Rev. B **53**, 12 502 (1996).

[11] Y. Wang, H. Rushan, and Z.-B. Su, Phys. Rev. B **50**, 10 350 (1994).

[12] S. Uma, T. Sarkar, K. Sethupathi, M. Seshasayee, G. Rangarajan, C. Changkang, H. Yongle, B. M. Wanklyn, and J. W. Hodby, Phys. Rev. B **53**, 6829 (1996).

[13] R. A. Fisher, N. E. Phillips, D. A. Wright, H. B. Radousky, T. J. Goodwin, J. L. Peng, R. N. Shelton, and L. Zhang, Physica C **235-240**, 1749 (1994).

[14] P. Lundqvist, C. Tengroth, Ö. Rapp, R. Tellgren, and Z. Hegedüs, Physica C **269**, 231 (1996).

[15] G. Hilscher, E. Holland-Moritz, T. Holubar, H.-D. Jostarndt, V. Nekvasil, G. Schaudy, U. Walter, and G. Fillion, Phys. Rev. B **49**, 535 (1994).

[16] A. T. Boothroyd, S. M. Doyle, and R. Osborn, Physica C **217**, 425 (1993).

[17] K. Nehrke, M. W. Pieper, and T. Wolf, Phys. Rev. B **53**, 1 (1996).

[18] K. Nehrke and M. W. Pieper, Phys. Rev. Lett. **76**, 1936 (1996).

[19] M. E. Lopez-Morales, D. Rios-Jara, J. Tagüena, R. Escudero, S. L. Placa, A. Bezinge, V. Y. Lee, E. M. Engler, and P. M. Grant, Phys. Rev. B **41**, 6655 (1990).

[20] J. Fink, N. Nücker, H. Romberg, M. Alexander, M. B. Maple, J. J. Neumeier, and J. W. Allen, Phys. Rev. B **42**, 4823 (1990).

[21] A. Hartmann, G. J. Russell, W. Fentrup, and K. N. R. Taylor, Solid State Commun. **89**, 77 (1994).

[22] R. Fehrenbacher and T. M. Rice, Phys. Rev. Lett. **70**, 3471 (1993).

[23] A. I. Liechtenstein and I. I. Mazin, Phys. Rev. Lett. **74**, 1000 (1995).

[24] I. I. Mazin and A. I. Liechtenstein, Phys. Rev. B **57**, 150 (1998).

[25] D. Khomskii, J. Supercond. **6**, 69 (1993).

[26] S.-L. Drechsler, J. Malek, and H. Eschrig, Phys. Rev. B **55**, 606 (1997).

[27] M. Guillaume, P. Allenspach, W. Henggeler, J. Mesot, B. Roessli, U. Staub, P. Fischer, and A. Furrer, J. Phys.: Condens. Matter **6**, 7963 (1994).

[28] Z. Hu, R. Meier, C. Schüßler-Langeheine, E. Weschke, G. Kaindl, I. Felner, M. Merz, N. Nücker, S. Schuppler, and A. Erb, Phys. Rev. B **60**, 1460 (1999).

[29] J. M. Chen, R. S. Liu, J. G. Lin, C. Y. Huang, and J. C. Ho, Phys. Rev. B **55**, 14 586 (1997).

[30] M. Merz, N. Nücker, E. Pellegrin, P. Schweiss, S. Schuppler, M. Kielwein, M. Knupfer, M. S. Golden, J. Fink, C. T. Chen, V. Chakarian, Y. U. Idzerda, and A. Erb, Phys. Rev. B **55**, 9160 (1997).

[31] R. McCormack, D. de Fontaine, and G. Ceder, Phys. Rev. B **45**, 12 976 (1992).

[32] D. J. Liu, T. L. Einstein, P. A. Sterne, and L. T. Wille, Phys. Rev. B **52**, 9784 (1995).

[33] A. A. Aligia, J. Garces, and H. Bonadero, Physica C **190**, 234 (1992).

[34] I. Heinmaa, H. Lütgemeier, S. Pekker, G. Krabbes, and M. Buchgeister, Appl. Magn. Reson. **3**, 689 (1992).

[35] H. Lütgemeier, S. Schmenn, P. Meuffels, O. Storz, R. Schöllhorn, C. Niedermayer, I. Heinmaa, and Y. Baikov, Physica C **267**, 191 (1996).

[36] G. Uimin and J. Rossat-Mignod, Physica C **199**, 251 (1992).

[37] C. Ambrosch-Draxl, P. Blaha, and K. Schwarz, J. Phys. C **6**, 2347 (1994).

[38] T. Ohno, K. Koyama, and H. Yasuoka, Physica B **237-238**, 100 (1997).

[39] O. N. Bakharev, A. V. Dooglav, E. V. Egorov, H. Lütgemeier, M. P. Rodionova, M. A. Teplov, A. G. Volodin, and D. Wagener, Appl. Magn. Reson. **3**, 613 (1992).

[40] W.-H. Li, W. Lynn, S. Skanthakumar, and T. Clinton, Phys. Rev. B **40**, 5300 (1989).

[41] A. T. Boothroyd, A. Longmore, N. H. Andersen, E. Brecht, and T. Wolf, Phys. Rev. Lett. **78**, 130 (1997).

[42] S. Uma, W. Schnelle, E. Gmelin, G. Rangarajan, S. Skanthakumar, J. W. Lynn, R. Walter, T. Lorenz, B. Büchner, E. Walker, and A. Erb, J. Phys. C **10**, L33 (1998).

[43] U. Staub, Phys. Rev. Lett. **77**, 4688 (1996).

[44] D. W. Cooke, M. S. Jahan, R. S. Kwok, R. L. Lichti, T. R. Adams, C. Boekema, W. K. Dawson, A. Kebede, J. Schwegler, J. E. Crow, and T. Mihalisin, Hyperfine Interact. **63**, 213 (1990).

[45] A. Sundaresan, K. Ghosh, S. Ramakrishnan, L. C. Gupta, G. Chandra, M. Sharon, and R. Vijayaraghavan, Phys. Rev. B **49**, 6388 (1994).

[46] W. T. Hsieh, K. J. Chang, W.-H. Li, K. C. Lee, J. W. Lynn, C. C. Lai, and H. C. Ku, Phys. Rev. B **49**, 12 200 (1994).

[47] C. C. Lai, T. J. Lee, H. K. Fun, H. C. Ku, and J. C. Ho, Phys. Rev. B **50**, 4092 (1994).

[48] H. Drößler, H.-D. Jostarndt, J. Harnischmacher, J. Kalenborn, U. Walter, A. Severing, W. Schlabitz, and E. Holland-Moritz, Z. Phys. B: Condens. Matter **100**, 1 (1996).

[49] W. Guan, Y. Xu, S. R. Sheen, Y. C. Chen, J. Y. T. Wei, H. F. Lai, M. K. Wu, and J. C. Ho, Phys. Rev. B **49**, 15 993 (1994).

[50] I. Das, E. V. Sampathkumaran, R. Vijayaraghavan, Y. Nakazawa, and M. Ishikawa, Physica C **173**, 331 (1991).

[51] A. Kebede, C. S. Jee, J. Schwegler, J. E. Crow, T. M. G. H. Myer, R. E. Salomon, P. Schlottmann, M. V. Kuric, S. H. Bloom, and R. P. Guertin, Phys. Rev. B **40**, 4453 (1989).

[52] Z. Zou, K. Oka, T. Ito, and Y. Nishihara, Phys. Rev. Lett. **80**, 1074 (1998).

[53] M. Luszczek, W. Sadowski, T. Klimczuk, J. Olchowik, B. Susla, and R. Czaijka, Physica C **322**, 57 (1999).

[54] K. Widder, M. Merz, D. Berner, J. Münzel, H. P. Geserich, A. Erb, R. Flükiger, W. Widder, and H. F. Braun, Physica C **264**, 11 (1996).

[55] E. Brecht, W. W. Schmahl, H. Fuess, S. Schmenn, H. Lütgemeier, N. H. Andersen, B. Lebech, and T. Wolf, Phys. Rev. B **56**, 940 (1997).

[56] M. Tagami, M. Sumida, C. Krauns, Y. Yamada, T. Umeda, and Y. Shiohara, Physica C **250**, 240 (1995).

[57] M. Park, M. J. Kramer, K. W. Dennis, and R. W. McCallum, Physica C **259**, 43 (1996).

[58] M. Tagami and Y. Shiohara, J. Cryst. Growth **171**, 409 (1997).

[59] T. B. Lindemer, B. C. Chakoumakos, E. D. Specht, R. K. Williams, and Y. J. Chen, Physica C **231**, 80 (1994).

[60] C. Bertrand, P. Galez, R. E. Gladyshevskii, and J. L. Jorda, Physica C **321**, 151 (1999).

[61] T. Wolf, W. Goldacker, B. Obst, G. Roth, and R. Flükiger, J. Cryst. Growth **96**, 1010 (1989).

[62] C. Changkang, A. T. Boothroyd, H. Yongle, F. R. Wondre, B. M. Wanklyn, and J. W. Hodby, Physica C **214**, 231 (1994).

[63] A. J. Markvardsen, A. T. Boothroyd, B. Buck, G. J. McIntyre, and T. Wolf, J. Magn. Magn. Mater. **177-181**, 502 (1998).

[64] M. J. Kramer, K. W. Dennis, D. Falzgraf, R. W. McCallum, S. K. Malik, and W. B. Yelon, Phys. Rev. B **56**, 5512 (1997).

[65] C. H. Booth, F. Bridges, J. B. Boyce, T. Claeson, Z. X. Zhao, and P. Cervantes, Phys. Rev. B **49**, 3432 (1994).

[66] H. D. Yang, M. W. Lin, C. K. Chiou, and W. H. Lee, Phys. Rev. B **46**, 1176 (1992).

[67] B. Fisher, G. Koren, J. Genossar, L. Patlagan, and E. L. Gartstein, Physica C **176**, 75 (1991).

[68] J. Yoshida and T. Nagamo, Phys. Rev. B **55**, 11 860 (1997).

[69] M. J. Kramer, S. I. Yoo, R. W. McCallum, W. B. Yelon, H. Xie, and P. Allenspach, Physica C **219**, 145 (1994).

[70] S. Uma, W. Schnelle, E. Gmelin, G. Rangarajan, and A. Erb, J. Appl. Phys. **81**, 4227 (1997).

[71] N. H. Andersen and G. Uimin, Phys. Rev. B **56**, 10 840 (1997).

[72] A. Longmore, A. T. Boothroyd, C. Changkang, H. Yongle, M. P. Nutley, N. H. Andersen, H. Casalta, P. Schleger, and A. N. Christensen, Phys. Rev. B **53**, 9382 (1996).

[73] A. T. Boothroyd, J. M. Reynolds, N. H. Andersen, E. Brecht, T. Wolf, and A. J. S. Chowdhury, Phys. Rev. B **60**, 1400 (1999).

[74] N. Rosov, J. Lynn, G. Cao, J. O'Reilly, P. Pernambuco-Wise, and J. Crow, Physica C **204**, 171 (1992).

[75] B. Grevin, Y. Berthier, G. Collin, and P. Mendels, Phys. Rev. Lett. **80**, 2405 (1998).

[76] Z. Zou, K. Oka, T. Ito, and Y. Nishihara, Jpn. J. Appl. Phys., Part 2 **36**, L18 (1997).

[77] H. A. Blackstead, D. B. Chrisey, J. D. Dow, J. S. Horwitz, A. E. Klunzinger, and D. B. Pulling, Phys. Lett. A **207**, 109 (1995).

[78] V. N. Narozhnyi, D. Eckert, K. A. Nenkov, G. Fuchs, K.-H. Müller, and T. G. Uvarova, Int. J. Mod. Phys. B **13**, 3712 (1999).

[79] A. A. Moolenaar, P. C. M. Gubbens, J. J. van Loef, M. J. V.

Menken, and A. A. Menovsky, Hyperfine Interact. **93**, 1717 (1994).

[80] V. N. Narozhnyi, D. Eckert, K. A. Nenkov, G. Fuchs, T. G. Uvarova, and K.-H. Müller, Physica C **312**, 233 (1999).

[81] K. Nehrke, Ph.D. thesis, Universität Hamburg, 1996 (in German).

[82] D. J. Singh, K. Schwarz, and P. Blaha, Phys. Rev. B **46**, 5849 (1992).

[83] S. Schmenn, Ph.D. thesis, FZ-Juelich, 1996 (in German).

[84] P. Allenspach, J. Mesot, U. Staub, M. Guillaume, A. Furrer, S.-I. Yoo, M. J. Kramer, R. W. McCallum, H. Maletta, H. Blank, H. Mutka, R. Osborn, M. Arai, Z. Bowden, and A. D. Taylor, Z. Phys. B: Condens. Matter **95**, 301 (1994).

[85] A. Trokiner, L. L. Noc, K. Mikhalev, A. Yakubovski, H. Lütge-meier, I. Heinmaa, A. Gippius, S. Verkhovskii, D. Goldschmidt, and Y. Eckstein, Physica C **226**, 43 (1994).

[86] B. Bleaney, in *Magnetic Properties of Rare Earth Metals*, edited by R. J. Elliott (Plenum Press, New York, 1972), p. 383.

[87] M. A. H. McCausland and I. S. Mackenzie, Adv. Phys. **28**, 305 (1979).

[88] M. T. Hutchings, in *Solid State Physics*, edited by F. Seitz and D. Turnbull (Academic Press, New York, 1964), Vol. 16, p. 227.

[89] A. J. Kassman, J. Chem. Phys. **53**, 4118 (1970).

[90] K. R. Lea, M. J. M. Leask, and W. P. Wolf, J. Phys. Chem. Solids **23**, 1381 (1962).

[91] J. A. Hodges, G. le Bras, P. Bonville, P. Imbert, and G. Jehanno, Physica C **218**, 283 (1993).

[92] W.-H. Li, W. T. Hsieh, S. T. Shyr, K. C. Lee, J. H. Shieh, and H. C. Ku, Physica B **206-207**, 753 (1995).